Materials Today Bio 24 (2024) 100903

Contents lists available at ScienceDirect

Materials Today Bio

journal homepage: www.journals.elsevier.com/materials-today-bio

Morphologically transformable peptide nanocarriers coloaded with doxorubicin and curcumin inhibit the growth and metastasis of hepatocellular carcinoma

Yun Liu [a,1], Yunxia Liu [a,b,1], Xinyu Sun [c], Yue Wang [c], Changqing Du [b], Jingkun Bai [d,*]

[a] School of Stomatology, Weifang Medical University, Weifang, 261053, China
[b] Department of Dentistry, Affiliated Hospital of Weifang Medical University, Weifang, 261035, China
[c] School of Medical Sciences, Weifang Medical University, Weifang, 261053, China
[d] School of Bioscience and Technology, Weifang Medical University, Weifang, 261053, China

ARTICLE INFO

Keywords:
Peptide self-assembly
CREKA targeting
pH responsive
Morphological transformation
Drug retention

ABSTRACT

In tumor treatment, the highly disordered vascular system and lack of accumulation of chemotherapeutic drugs in tumors severely limit the therapeutic role of nanocarriers. Smaller drug-containing nanoparticles (NPs) can better penetrate the tumor but are easily removed, which severely limits the tumor-killing properties of the drug. The chemotherapeutic medication doxorubicin (DOX) is highly toxic to the heart, but this toxicity can be effectively mitigated and the combined anticancer effect can be enhanced by clinically incorporating curcumin (CUR) as part of the dual therapy. We designed a small-molecule peptide, Pep1, containing a targeting peptide (CREKA) and a pH-responsive moiety. These NPs can target the blood vessels in tumor microthrombi and undergo a morphological shift in the tumor microenvironment. This process enhances the penetration and accumulation of drugs, ultimately improving the effectiveness of cancer treatment. *In vitro* and *in vivo* experiments demonstrated that this morphological transformation allowed rapid and effective drug release into tumors, the effective inhibition of tumor angiogenesis, and the promotion of tumor cell apoptosis, thus effectively killing tumor cells. Our findings provide a novel and simple approach to nhibit the growth and metastasis of hepatocellular carcinoma.

1. Introduction

Hepatocellular carcinoma (HCC) is of concern for its high incidence and mortality worldwide [1]. Chemotherapy is the main modality of HCC treatment [2]. Rapid drug clearance is one of the factors that limits the effectiveness of current anticancer drugs [3]. Despite the efforts of scientists in developing nanodrug delivery systems to mitigate the harmful impacts of chemotherapeutic medications and enable drug penetration through the distinctive enhanced permeability and retention (EPR) effect of nanodrug carriers [4,5], attaining heightened drug accumulation and successful tumor suppression remains a challenging task. The drug-loaded systems self-assemble into small nanospheres that are more readily absorbed by tumors [6]. The duration of nanocarriers in tumors can be prolonged by morphological transition to a high aspect ratio, further extending the drug action time and achieving better antitumor effects [7–14]. Therefore, one possibility for solving the above problem is to design a spherical drug-loaded system that undergoes a morphological transformation to a high aspect ratio after reaching the tumor site. Primary structural alterations under the action of plasma amine oxidase (PAO) [15] or alkaline phosphatase (ALP) [16] reduce the intermolecular electrostatic repulsion, and the self-assembled peptides are transformed from spherical nanoparticles to nanofibers. Moreover, the tumor microenvironment is slightly acidic [17–19]. After drug-loaded peptides reach the tumor site, the electrostatic repulsion between peptide molecules decreases with decreasing solution pH, which is also expected to induce a morphological transformation. Yang et al. constructed a novel nanosystem of multitransformable MSNs@GO for the efficient loading and delivery of doxorubicin (DOX), in which the nanocarriers can achieve charge reversal and size reduction through acid-cleavable dynamic boronate bonds in an acidic microenvironment

* Corresponding author.
E-mail address: jkbaizg@163.com (J. Bai).
[1] These authors contributed equally to this work.

https://doi.org/10.1016/j.mtbio.2023.100903
Received 23 September 2023; Received in revised form 3 November 2023; Accepted 3 December 2023
Available online 12 December 2023

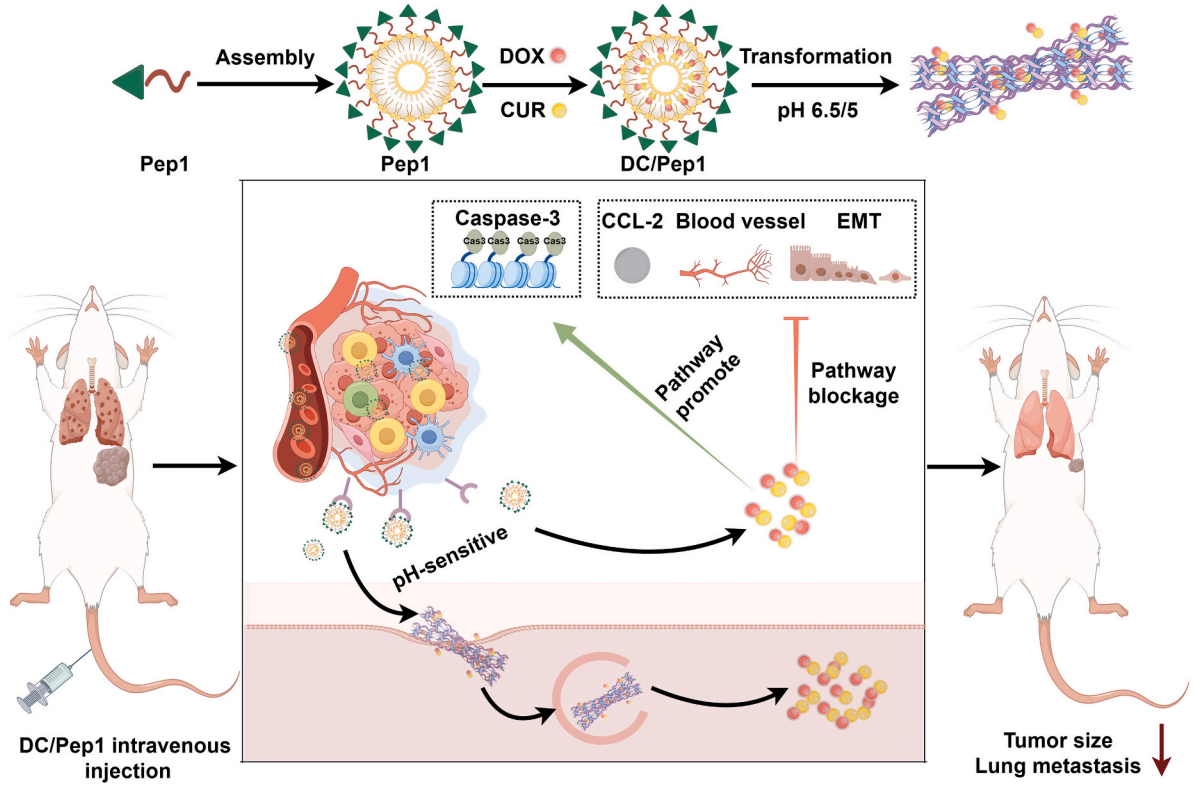

Fig. 1. Novel NPs of DC/Pep1 for Cancer Therapy. Pep1 encapsulated with DOX and CUR can self-assemble to form NPs (DC/Pep1), which can be targeted to the tumor vasculature and enter the tumor microenvironment in the presence of CREKA. DC/Pep1 undergoes morphological transformations in the acidic tumor microenvironment, resulting in drug release and prolonging drug retention in the tumor tissues *in vivo*. DC/Pep1 inhibits angiogenesis, promotes apoptosis, and inhibits C–C motif chemokine ligand-2 (CCL-2), resulting in effective inhibition of lung metastasis and synergistic antitumor effects (by Figdraw).

[20].

In the progression of HCC, the tumor vasculature provides sufficient nutrients and oxygen for tumor cell growth [21]. Therefore, researchers have developed various clinical approaches for treating tumors by targeting tumor blood vessels, including embolization strategies [22,23], vascular disruptors [24], and VEGF antibodies [25], with the aim of obstructing or suppressing the tumor vasculature. These clinical strategies confirm that the tumor vasculature is a tempting target for tumor therapy. In tumor blood vessels, the pentapeptide Cys-Arg-Glu-Lys-Ala (CREKA) specifically identifies coagulation plasma proteins. It is specifically highly expressed in many diseases [26], including metastatic cancer and angiogenic processes in thrombosis [27]. Researchers have found that the peptide CREKA can target tumors, enable accurate experimental tracking of ultrasmall breast cancer metastases [28], and participate in the formation of vascular-targeted drug delivery systems [27,29]. Several diseases have been imaged and treated using nanoplatforms based on CREKA. These findings have led to the development of CREKA-targeted peptides with the potential to serve as a specific and practical approach to block tumor angiogenesis.

DOX is a commonly used chemotherapeutic employed for treating HCC that inhibits DNA synthesis and thus tumor cell proliferation [29–32]. However, DOX can produce serious toxic side effects, including cardiotoxicity and nephrotoxicity [31]. Chemotherapy drugs administered alone have multiple disadvantages, including high toxicity and limited clinical efficacy [33]. Therefore, combining two or more drugs from different anticancer pathways is an increasingly important approach to improving anticancer outcomes and reducing toxicity [34]. Curcumin (CUR) promotes tumor apoptosis [35] and inhibits angiogenesis [36]. The conventional chemotherapeutic drug DOX was combined with the natural compound CUR to achieve a better tumor suppression effect.

Here, we used the amphiphilic small molecule peptide Pep1 as a nanocarrier to encapsulate DOX and CUR (DC/Pep1) through hydrophobic interactions to maximize the synergistic effects of chemotherapy and chemosensitization [37]. Inspired by the specific tumor microenvironment, small-molecule peptides containing both pH-responsive and vascular targeting motifs in microthrombi that are specific to target tumor vessels were designed and prepared. DC/Pep1 self-assembled into spherical nanoparticles (NPs), which ultimately transformed into aggregates with high aspect ratios in an acidic environment. The deformed drug-loaded peptides release CUR and DOX upon reaching tumor vessels, which inhibits tumor neovascularization and promotes tumor cell apoptosis. In addition, the morphological transformation ability of small molecule peptides can prolong drug retention within the tumor and achieve good antitumor effects (Fig. 1).

2. Materials and methods

2.1. Materials

DOX was purchased from APExBIO Technology LLC (Houston, USA), and CUR was purchased from Aladdin (Shanghai, China). CCK-8 kits were purchased from Dojindo Laboratories (Kumamoto, Japan). Fetal bovine serum (FBS) was purchased from Corning (VA, USA), and DAPI was purchased from Beyotime Biotechnology Co., Ltd. (Shanghai, China). The human hepatocellular carcinoma cell line HepG2 was provided by the American Type Culture Collection (ATCC). Human umbilical vein endothelial cells (HUVECs) and mouse H22 hepatocarcinoma (H22) cells were provided by BeNa Culture Collection (BNCC). HepG2 cells and HUVECs were inoculated in DMEM (pH 7.4) containing 10 % (v/v) FBS and cultured at 37 °C under 5 % CO_2. BALB/c mice were purchased from Pengyue Experimental Animal Breeding Co. Ltd. (Jinan, China).

2.2. Peptide self-assembly

The peptides and drug-loaded peptides dissolved in HEPES were added to the surface of the copper meshs, and a Hitachi HT7700 apparatus (Tokyo, Japan) was used to examine the peptide samples after they had dried naturally [38,39].

2.3. Zeta potential measurements

Using a Zetasizer Nano ZS90 instrument (Malvern Instruments, UK), the samples' zeta potentials were determined. Measurements were taken to determine the zeta potentials of Pep1 and Pep2. After DOX and CUR were encapsulated, DC/Pep1 and DC/Pep2 were allowed to stand at room temperature for 12 h and then evaluated. Subsequently, acid was introduced to the peptide solutions, and the potentials were measured following 12 h and 120 h of reaction at room temperature.

2.4. Cell counting Kit-8 (CCK-8) assay

The CCK-8 assay was used to measure how Pep1 and Pep2 affected the viability of HUVECs and HepG2 cells. We added 5×10^3 cells to each well.

In the various experimental groups, drugs were added to a serum-free HEPES buffer/peptide solution at a 1:1 ratio. The mixture was then incubated for 48 h. A microplate reader (Thermo Science, USA) was utilized to measure the optical density (OD) of the samples at 450 nm after a certain amount of time had passed after the addition of the CCK-8 reagent, and the percentage of cells that had survived in each group was determined.

2.5. Cellular uptake

The uptake of different medications by tumor cells was monitored using confocal laser scanning microscopy (CLSM) and flow cytometry (FCM). Following the addition of DC, DC/Pep2 or DC/Pep1 to each well (in a volume equal to 1/20 of the volume of the cell culture medium), HepG2 cells were cocultured for 0.25 h and 0.5 h. After this, the cells were stained with DAPI (1 μg/mL). The spatial distribution of DOX and CUR within the cells was determined by CLSM (TCS SP8, Leica, Germany), while fluorescence was quantified by ImageJ.

2.6. Apoptosis assay

Each well of a 6-well plate was seeded with approximately 5×10^5 HepG2 cells. Blank medium, Pep1, Pep2, DC, DOX/Pep2, DOX/Pep1, DC/Pep2 or DC/Pep1 (1/2500) were added to the 6-well plate according to the experimental grouping. After digestion and centrifugation of the cells, a total of 195 μL of Annexin V-FITC conjugate was introduced to carefully mix the cells. Then, 5 μL of Annexin V-FITC and 10 μL of PI staining solution were added. The mixture was allowed to incubate for 0.25 h in an area shielded from light before analysis by FCM.

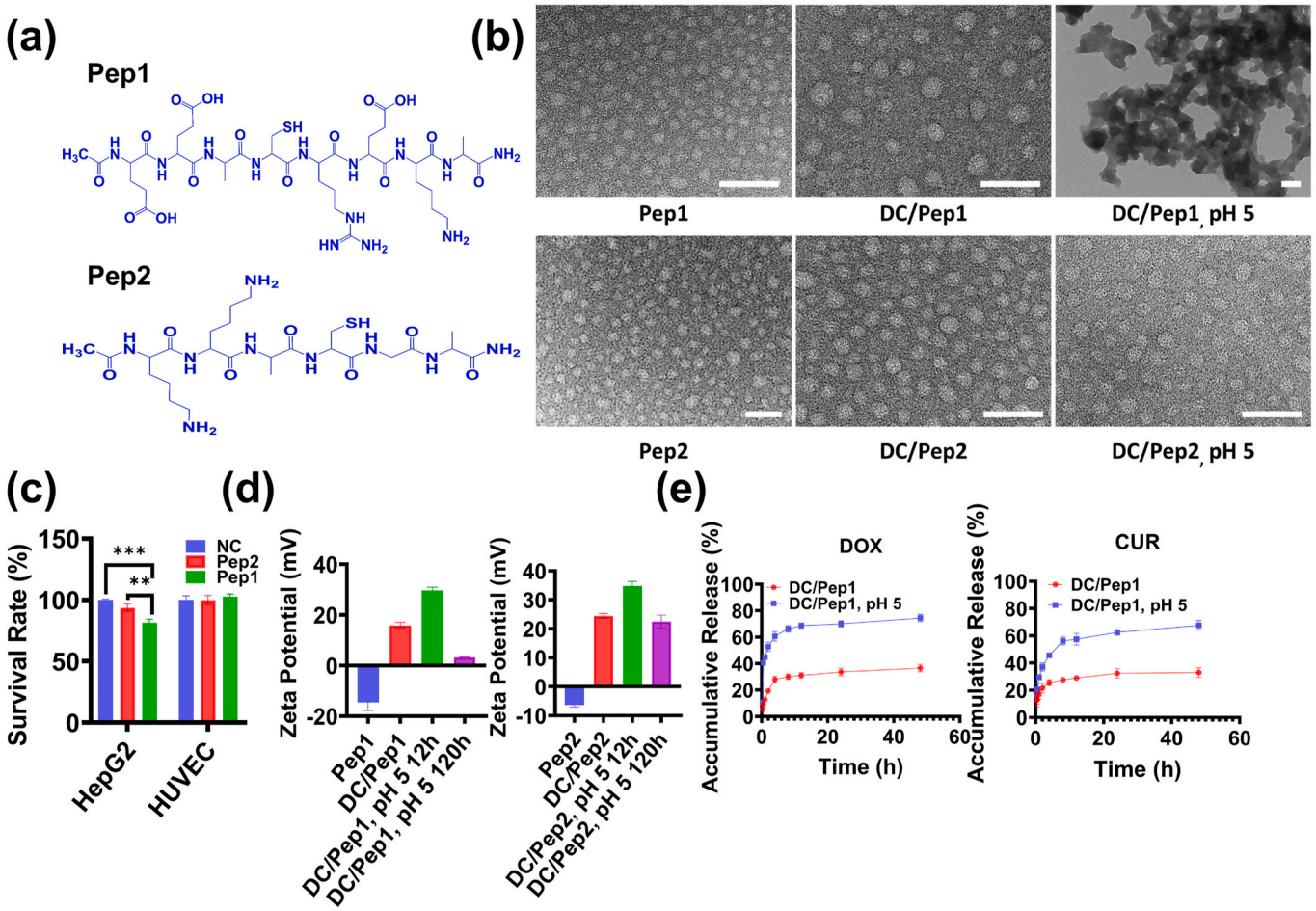

Fig. 2. Characterization and Cytotoxicity Assay of Peptides. (a) Structures of Pep1 and Pep2. (b) TEM images of Pep1, DC/Pep1, DC/Pep1 (pH 5), Pep2, DC/Pep2, and DC/Pep2 (pH 5). Scale bar: 100 nm. (c) Viability of HepG2 cells and HUVECs after 48 h of peptide treatment. $^{**}P < 0.01$; $^{***}P < 0.001$. (d) Changes in the zeta potentials of Pep1, DC/Pep1 and DC/Pep1 at pH 5 after 12 h and 120 h and the changes in Pep2 potential after the same treatments. (e) Cumulative DOX and CUR release profiles from Pep1 before and after the addition of acid.

2.7. Angiogenesis assays

In each well of the 48-well plates, 100 μL of Matrigel mixture (Matrigel: DMEM = 1:1) was added, and then 5×10^4 HUVECs that were spiked/treated were inoculated. After 3 h at 37 °C, tube formation was observed with an inverted fluorescence microscope. One random location per sample was used to count the number of tubes for comparison among groups.

2.8. Western blot (WB) analysis

Incubated cells were treated with serum-free medium, Pep1, Pep2, DC, DOX/Pep2, DOX/Pep1, DC/Pep2, or DC/Pep1 for 24 h. RIPA lysis buffer was used to extract total protein from cells. SDS–PAGE was used to isolate and transfer 20 μg protein samples onto 0.45 μm PVDF membranes. E-cadherin (dilution 1:1000, Beyotime), Vimentin (dilution 1:3000, Beyotime), Caspase-3 (dilution 1:3000, Beyotime), and β-actin (dilution 1:3000, Beyotime) rabbit monoclonal antibodies were added for incubation overnight at 4 °C after blocking. Samples were incubated with secondary antibodies coupled with horseradish peroxidase (HRP) at a dilution of 1:1000 (Beyotime) for a period of 1–2 h, followed by development using enhanced chemiluminescence (ECL) reagents.

2.9. In vivo live animal imaging

All experiments involving animals were performed in accordance with the guidelines of the Institutional Animal Care and Use Committee of Weifang Medical University. BALB/c mice were subcutaneously implanted with H22 cells at a concentration of 1×10^6 cells per mouse. When the tumor volume of BALB/c mice reached 100 mm^3, mice in randomly assigned groups (n = 3) were injected with the same concentration (40 μg/mL) of DiR, DiR/Pep2, and DiR/Pep1 (0.1 mL per mouse) through the tail vein. At 1, 4, 8, 12, 24, 48, 72 and 96 h, the drug distribution *in vivo* was measured using a small animal imaging device (IVIS Spectrum, PerkinElmer, USA) for live animal imaging. After 96 h, the mice were sacrificed, and their tumors and other vital organs were retrieved for *ex vivo* fluorescence imaging. Fluorescent readings were conducted by excitation at a wavelength of 745 nm and the detection of emissions at 835 nm.

2.10. In vivo antitumor activity

To assess the *in vivo* antitumor efficacy of various agents, mice with H22 tumors were generated. Once the tumors reached a volume of 100 mm^3, the mice were divided into six groups in a randomized manner (n = 6). Therapeutic drugs (DOX, 3 mg/kg; CUR, 0.75 mg/kg) were injected into the mice in the treated groups (saline, DC, DOX/Pep2, DOX/Pep1, DC/Pep2, DC/Pep1) via the tail vein every other day for 14 days starting on day 6. The tumor sizes and mouse body weights were measured every other day. Vernier calipers were used to measure the tumor dimensions, and tumors were weighed according to the method described previously [16,40,41].

2.11. Lung metastasis experiment

By injecting H22 cells (10^6 cells/mouse) via the tail vein, a lung metastasis model in BALB/c mice was established. Mice (n = 5) were randomly assigned to receive saline, DC, DOX/Pep2, DOX/Pep1, DC/Pep2, or DC/Pep1 intravenously once every two days. After 9 days of treatment, the organs of the mice were dissected. The number of metastatic nodules in the lungs was counted after collecting and photographing the lung tissue. Tissue immunofluorescence staining was performed on CCL-2-positive lung tissue sections to analyze the metastasis rate. Lung histopathology was visualized by conducting H&E staining on sections of the lung.

2.12. Statistical analysis

GraphPad Prism v6.0 (GraphPad Software) was used for all statistical analyses. We conducted statistical comparisons utilizing either Student's unpaired *t*-test or 2-way analysis of variance (ANOVA).

3. Results

3.1. pH-mediated morphological transformation of Pep1

The amphipathic peptide Pep1 containing the microthrombotic vascular targeting peptide sequence CREKA and glutamate was designed to encapsulate a refractory chemotherapeutic drug (Fig. 2a). The peptide Pep2 without the targeting peptide sequence was designed as a control (Fig. 2a). The purities of the synthesized peptides were greater than 95 % (Figs. S1–S4).

Transmission electron microscopy (TEM) was used to observe morphological changes in the peptides and drug-loaded peptides. Pep1 self-assembled to form spherical NPs in HEPES buffer (25 mM, pH 7.4) (Fig. 2b, Figs. S5,S6). DOX and CUR were encapsulated in the hydrophobic core of the nanocarriers, which retained their NP structures (Fig. 2b, Figs. S7-S10) [42,43]. Tumor tissues are usually acidic [44]. Interestingly, when the pH was adjusted to 5, the regular NPs disappeared, and fibrous aggregates with a high aspect ratio formed, whereas the morphology of DC/Pep2 remained largely unaltered (Fig. 2b, Fig. S11). DC/Pep1 underwent a morphological transition from NPs to aggregates with a high aspect ratio at pH 6.5, while DC/Pep2 remained in the form of spherical NPs (Figs. S12, S13, S14).

3.2. Cell toxicity of and drug release from drug-loaded Pep1

After HUVECs and HepG2 cells were cocultured with Pep2 and Pep1, respectively, both groups showed high cell viability with survival rates greater than 80 % (Fig. 2c, Fig. S15). There was a difference in the toxicity of Pep1 and Pep2 on HepG2 cells, and the survival rate of HepG2 in the Pep2 group was 93.6 % after 48 h of coincubation. In comparison, the survival rate of HepG2 cells in the Pep1 group decreased to 81.4 % (Fig. 2c, Fig. S15), which may be related to the morphological transformation of Pep1 [45]. Pep1 exhibited inhibitory effects on tumor cell growth and showed low toxicity to normal mammalian cells.

DOX is widely utilized in cancer therapy, but it does not possess tumor-targeting capabilities [46]. Conventional DOX injection produces severe toxicity after intravenous administration [47]. CUR can promote tumor cell apoptosis but has low water solubility and bioavailability. Peptides can encapsulate drugs with low aqueous solubility in the hydrophobic core [48]. The potential of Pep1 was negative and the zeta potential of DC/Pep1 positive after encapsulation of DOX and CUR (Fig. 2d). The potential increased after adjustment to pH 5 and standing for 12 h. However, there was a significant decrease in the zeta potential of DC/Pep1 after standing for 120 h. With increasing time, the encapsulated drug may have been released from DC/Pep1, decreasing the zeta potential. This change in the zeta potential was also observed for Pep2 after its encapsulation of drugs and pH adjustment. However, there was no notable decrease in the zeta potential at pH 5 after 120 h (Fig. 2d). The zeta potential of Pep1 at pH 5 was lower than that of DC/Pep1 at pH 5 (Fig. S16), which indicated that some of the drugs remained in DC/Pep1 after DC/Pep1 the morphological transition.

Drug release experiments showed that DC/Pep1 released 74.5 % of loaded DOX and 67.7 % of loaded CUR in an acidic environment after 48 h (Fig. 2e). DC/Pep1 released 36.7 % DOX and 33.1 % CUR release in a neutral environment after 48 h (Fig. 2e). This result suggests that the drug can be released in response to an acidic environment, possibly caused by the morphological transformation of the Pep1 nanocarriers.

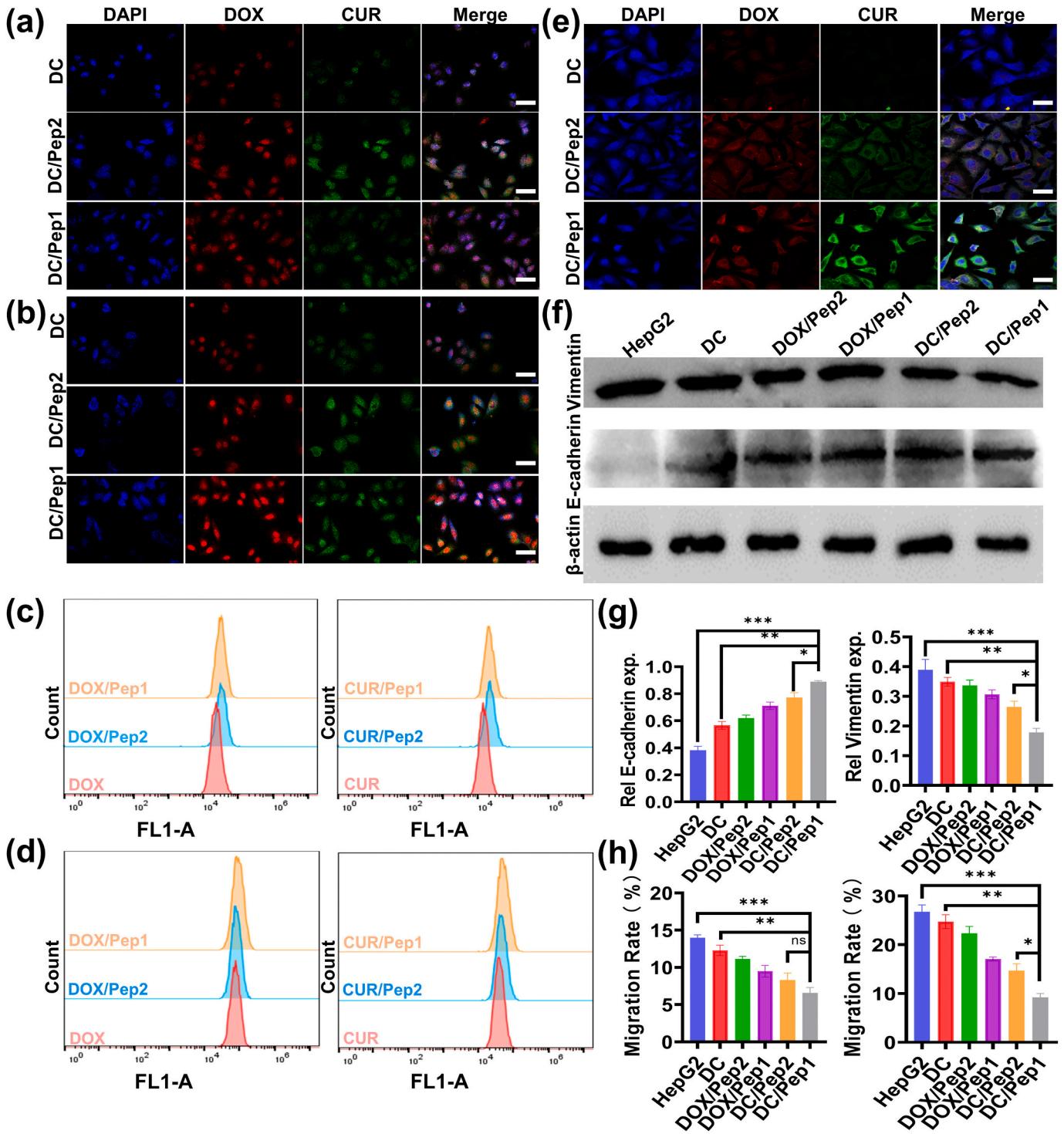

Fig. 3. Effects of Pep1 on Tumor Cell Uptake, Retention and Migration. CLSM images of HepG2 cells coexisting with DC, DC/Pep2, and DC/Pep1 for (a) 0.25 h and (b) 0.5 h. Scale bar: 50 μm. Uptake of DOX and CUR in HepG2 cells after coculture with DC, DC/Pep2, and DC/Pep1 for (c) 0.25 h and (d) 0.5 h was detected by FCM. (e) CLSM images of HepG2 cells cocultivated with DC, DC/Pep2, and DC/Pep1 for 72 h. Scale bar: 50 μm. (f) WB images indicating Vimentin and E-cadherin and (g) quantitative analysis. (h) Quantitative evaluation of HepG2 cells at 24 h and 48 h intervals following the scratch assay. *$P < 0.05$; **$P < 0.01$; ***$P < 0.001$; ns, $P > 0.05$ relative to DC/Pep1.

3.3. *In vitro effects of Pep1 on tumor cell uptake, retention and migration*

We further explored the capacity of tumor cells to take up the nanodrugs using the fluorescence properties of DOX and CUR. The uptake by HepG2 cells was investigated using CLSM and FCM. The positions of red and green fluorescence and their brightness indicate the stepwise uptake of DOX and CUR by the cells and their accumulation in CLSM images, respectively. HepG2 cells exhibited limited uptake of the free drug, while the cellular uptake significantly improved upon encapsulation of the medication within the nanocarriers. After 0.25 h of co-incubation, higher drug uptake was achieved for DC/Pep2 than DC/Pep1, possibly because the electropositivity of the drug-loaded peptide facilitated drug uptake [49–52] (Fig. 3a, Fig. S17). After 0.5 h of incubation, the DC/Pep1-treated cells showed intense green and red

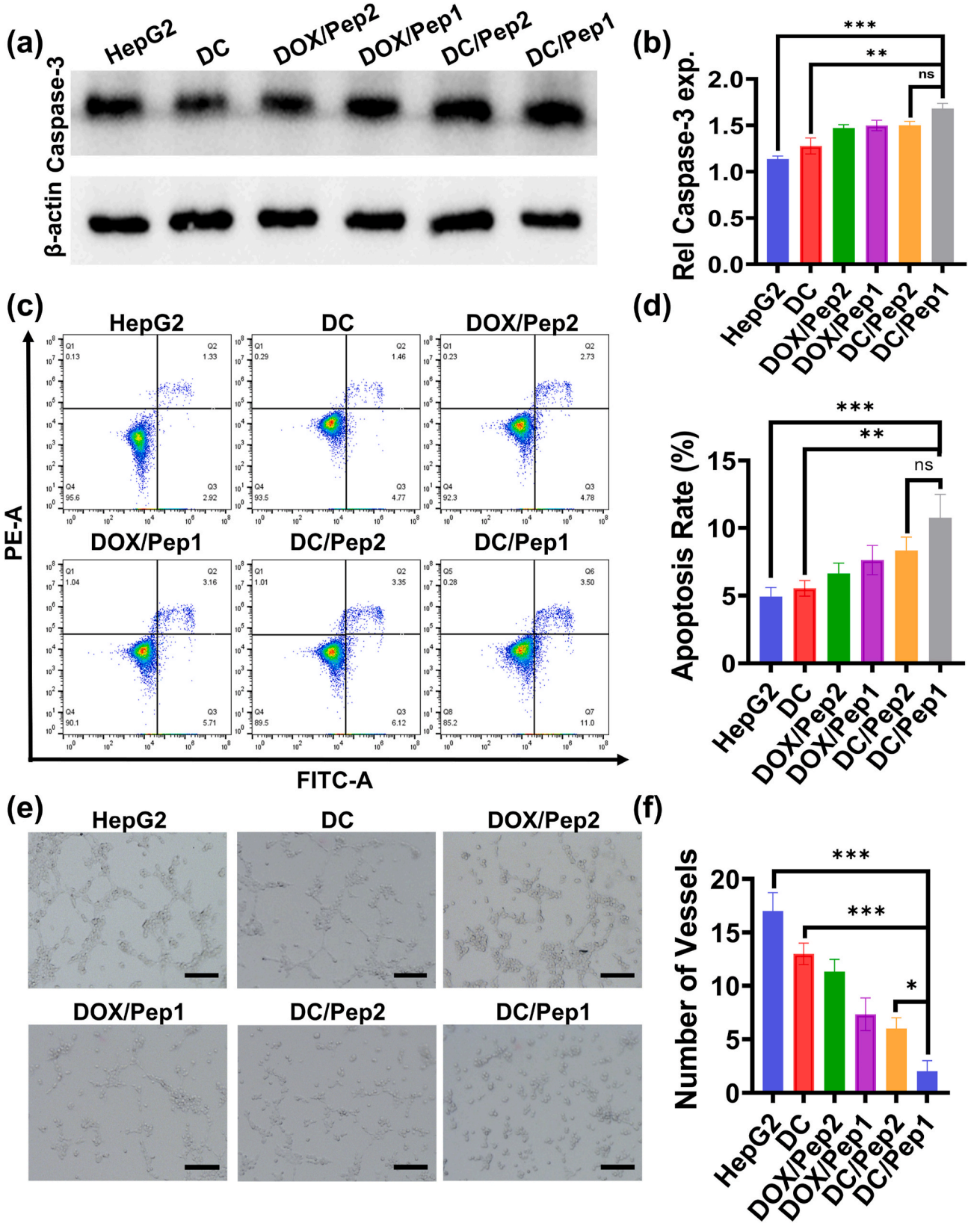

Fig. 4. Effects of Drug-loaded Peptides on HepG2 Cell Apoptosis and Angiogenesis. (a) WB analysis and (b) quantitative analysis of Caspase-3 activation. (c) Flow chart of HepG2 cell apoptosis (Q1: necrotic cells; Q2: late apoptotic cells; Q3: early apoptotic cells; and Q4: live cells) and (d) quantitative analysis. (e) Representative photographs and (f) quantitative analysis of the numbers of tubes formed and the capture of tubular structures in HUVECs. Scale bar: 200 μm. $^{*}P < 0.05$; $^{**}P < 0.01$; $^{***}P < 0.001$; ns, $P > 0.05$ relative to DC/Pep1.

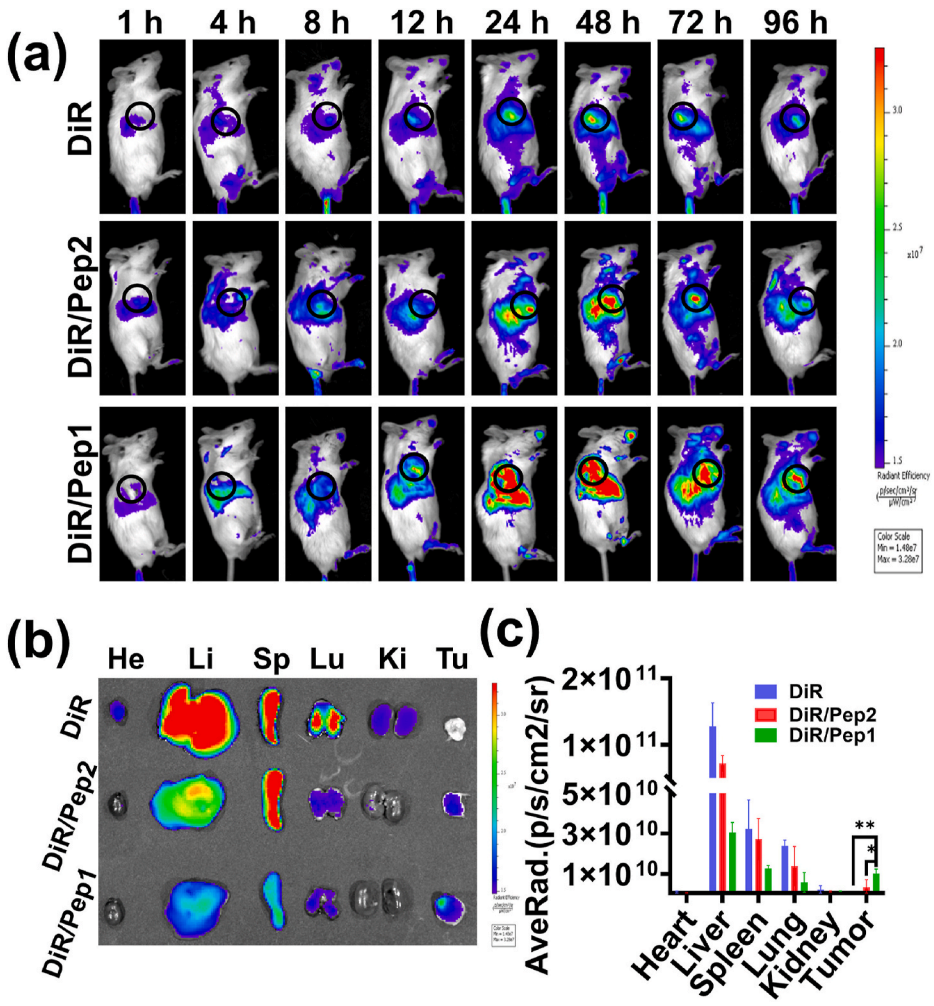

Fig. 5. Distribution of DiR in H22 Tumor-Bearing Mice *in Vivo* and in Isolated Tumors and Major Organs. (a) Fluorescence images of live mice were observed *in vivo* following the administration of DiR, DiR/Pep2 and DiR/Pep1 via intravenous injection during specific time intervals. (b) Fluorescence images of tissues *ex vivo* at the designated time intervals and (c) quantitative analysis. $^{*}P < 0.05$; $^{**}P < 0.01$.

fluorescence in the cytoplasmic and nuclear regions with increasing time, and portions of DOX and CUR were distributed in the nuclei (Fig. 3b, Fig. S18).

The uptake of drugs by HepG2 cells was analyzed using FCM after coincubation for 0.25 h and 0.5 h. After 0.25 h of incubation, the DC/Pep2 and DC/Pep1 groups showed higher intracellular fluorescence than the DC group. DC/Pep2 had slightly higher cellular uptake than DC/Pep1 after coincubation for 0.25 h (Fig. 3c, Figs. S19, S20). Subsequently, the distribution of DC/Pep1 in the cell gradually increased (Fig. 3d, Figs. S21, S22). Pep1 and Pep2 promoted the uptake of the encapsulated drug molecules into cells.

As chemotherapeutic drugs are readily eliminated by tumor cells [53], it is crucial to prolong drug retention within tumor cells. After 72 h of coincubation with DC, DC/Pep2 and DC/Pep1, confocal microscopy detected the red fluorescence of DOX and the green fluorescence of CUR in HepG2 cells. In the tumor cells, the drug-loaded peptide exhibited stronger red and green fluorescence signals than the DC group, and the fluorescence in the DC/Pep1 group was the most intense (Fig. 3e, Fig. S23). This finding suggests that DC/Pep1 prolongs the intracellular retention time and enhances drug accumulation capacity, which may be related to the morphological transformation of DC/Pep1.

Tumor metastasis relies heavily on epithelial-mesenchymal transition (EMT) [54]. During this process, epithelial adhesion molecules (such as E-cadherin) are downregulated, and mesenchymal markers (such as Vimentin) are upregulated [55]. WB experiments revealed that DC/Pep1 reduced Vimentin expression and increased E-cadherin levels in HepG2 cells compared to the control group (Fig. 3f and g). In the cell scratching experiments, HepG2 cells in the blank group displayed significant migration toward the central part of the scratch, and a small amount of migration was also observed in the DC and DC/Pep2 groups, while almost no migration was observed in the DC/Pep1 group (Fig. 3h, Fig. S24). Pep1 slightly affected EMT-related proteins and inhibited the migration of tumor cells (Figs. S25–S29). This may be related to the vascular targeting properties of Pep1.

3.4. DC/Pep1 enhances apoptosis and inhibits angiogenesis in tumor cells

Apoptosis is the process of autonomous and orderly cell death under genetic control [56]. Tumor cells undergo distinct proliferation and differentiation processes compared to normal cells, and they often exhibit defective or blocked apoptosis. Therefore, promoting apoptosis is a popular strategy for treating tumors [57]. Apoptosis is divided into endogenous and exogenous apoptosis, and Caspase-3 plays an indispensable role in the latter [58]. Pep1 showed increased Caspase-3 activity (Figs. S30 and S31) and a higher apoptosis rate than Pep2 (Figs. S32 and S33). Caspase-3 expression was elevated in the DC/Pep1 group compared with that in the HepG2, DC, DOX/Pep2, DOX/Pep1, and DC/Pep2 groups (Fig. 4a and b). DC/Pep1 can induce apoptosis by increasing apoptotic protein expression to inhibit tumor progression. We applied the FITC-Annexin V/PI double-staining technique to stain the

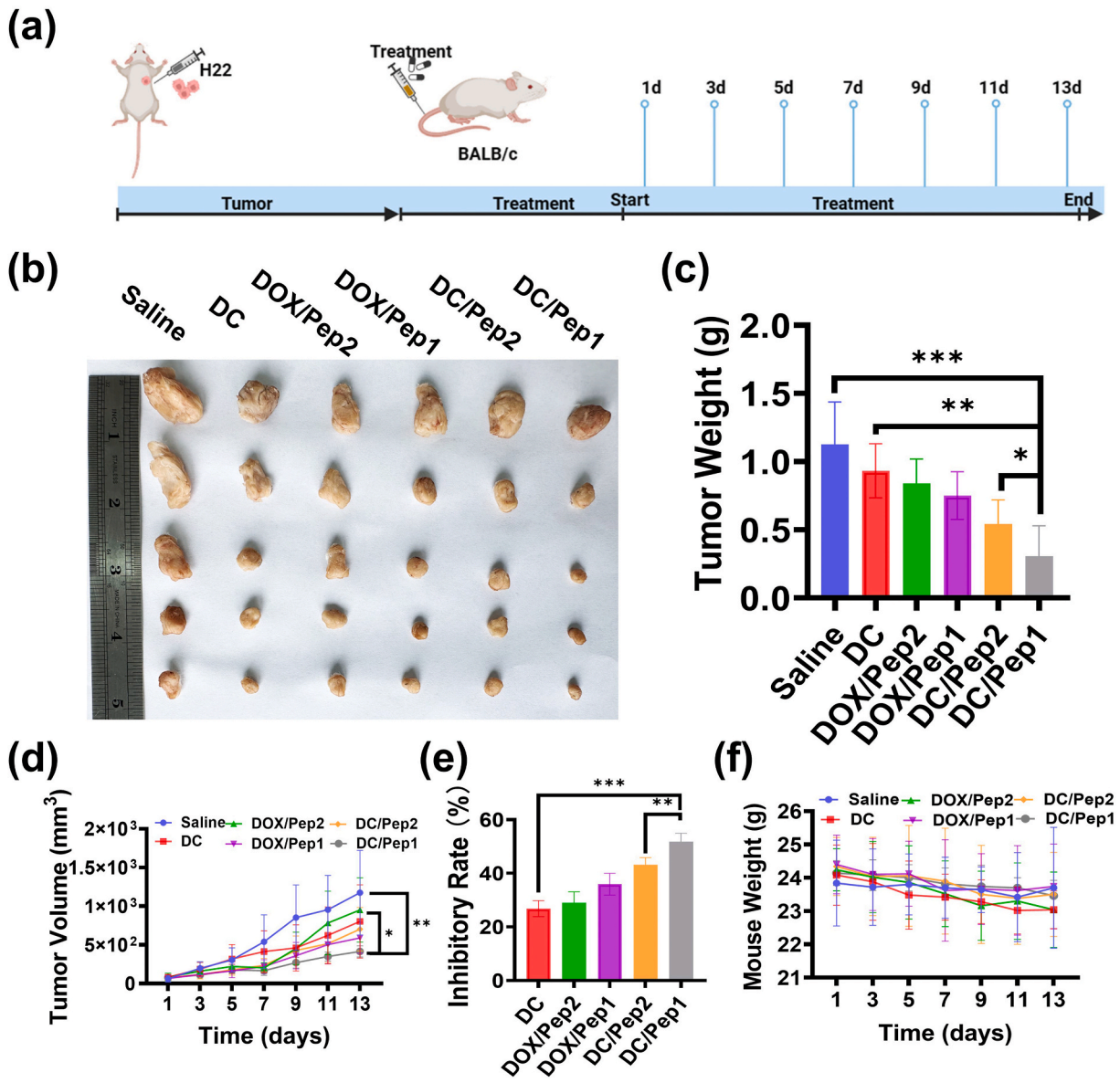

Fig. 6. *In Vivo* Antitumor Effects. (a) *In vivo* antitumor assay. (b) Images, (c) weights and (d) volumes of H22 tumors excised on day 14. (e) Rates of tumor inhibition achieved. (f) Differences in the weight of mice with tumors. *$P < 0.05$; **$P < 0.01$; ***$P < 0.001$.

cells, followed by employing FCM to measure the rate of apoptosis (Fig. 4c and d). The total apoptosis rates (early apoptosis and late apoptosis) induced in the HepG2, DC, DOX/Pep2, DOX/Pep1, DC/Pep2, and DC/Pep1 groups were 4.9 %, 5.5 %, 6.6 %, 7.6 %, 8.3 %, and 10.8 %, respectively. DC/Pep1 significantly increased the apoptosis rate compared to DOX/Pep2 and DC/Pep2. These results may be attributed to the prolonged duration of CUR, which in turn promotes apoptosis and synergistically enhances the antitumor effect of the chemotherapeutic drug DOX [59].

Adequate blood supply to the tumor site allows new blood vessels to form for growth and metastasis, contributing significantly to the development of the tumor [60]. We performed a stromal gel-based capillary formation assay using HUVECs to investigate whether drug-loaded peptides affect angiogenesis *in vitro*. Pep1 was more efficient at inhibiting angiogenesis than Pep2 (Figs. S34 and S35), which may be due to the targeting of Pep1. Significantly reduced angiogenesis was observed in the DC/Pep1 group compared with the other groups (Fig. 4e and f). DC/Pep1 effectively inhibited tumor blood vessel formation.

3.5. DC/Pep1 enhances the efficiency of in vivo tumor therapy

We investigated the *in vivo* retention properties of the drug-loaded peptide, and BALB/c mice bearing H22 subcutaneous tumors were established. After injecting DiR, DiR/Pep2, or DiR/Pep1 intravenously, live imaging was employed to track the dispersion of fluorescence in the mice. Only a minimal amount of fluorescence in the DiR group accumulated at the tumor location. The concentration of fluorescence in the DiR/Pep1 group was significantly higher at the tumor location. The most intense fluorescence was found 48 h after DiR/Pep1 NP injection, and a strong fluorescence signal was still present 96 h later (Fig. 5a). Mice were sacrificed 96 h after *in vivo* imaging to examine the distribution and intensity of the remaining DiR within each organ and tumor. We observed weaker fluorescence in normal organs but increased accumulation in tumor tissues after DiR/Pep1 treatment than after DiR and DiR/Pep2 treatment (Fig. 5b and c). This may because DiR/Pep1 exhibits passive targeting by the EPR effect [61], as well as CREKA-mediated microthrombus targeting [26]. Thus, it increases drug enrichment at the tumor site while decreasing its distribution in other organs. In

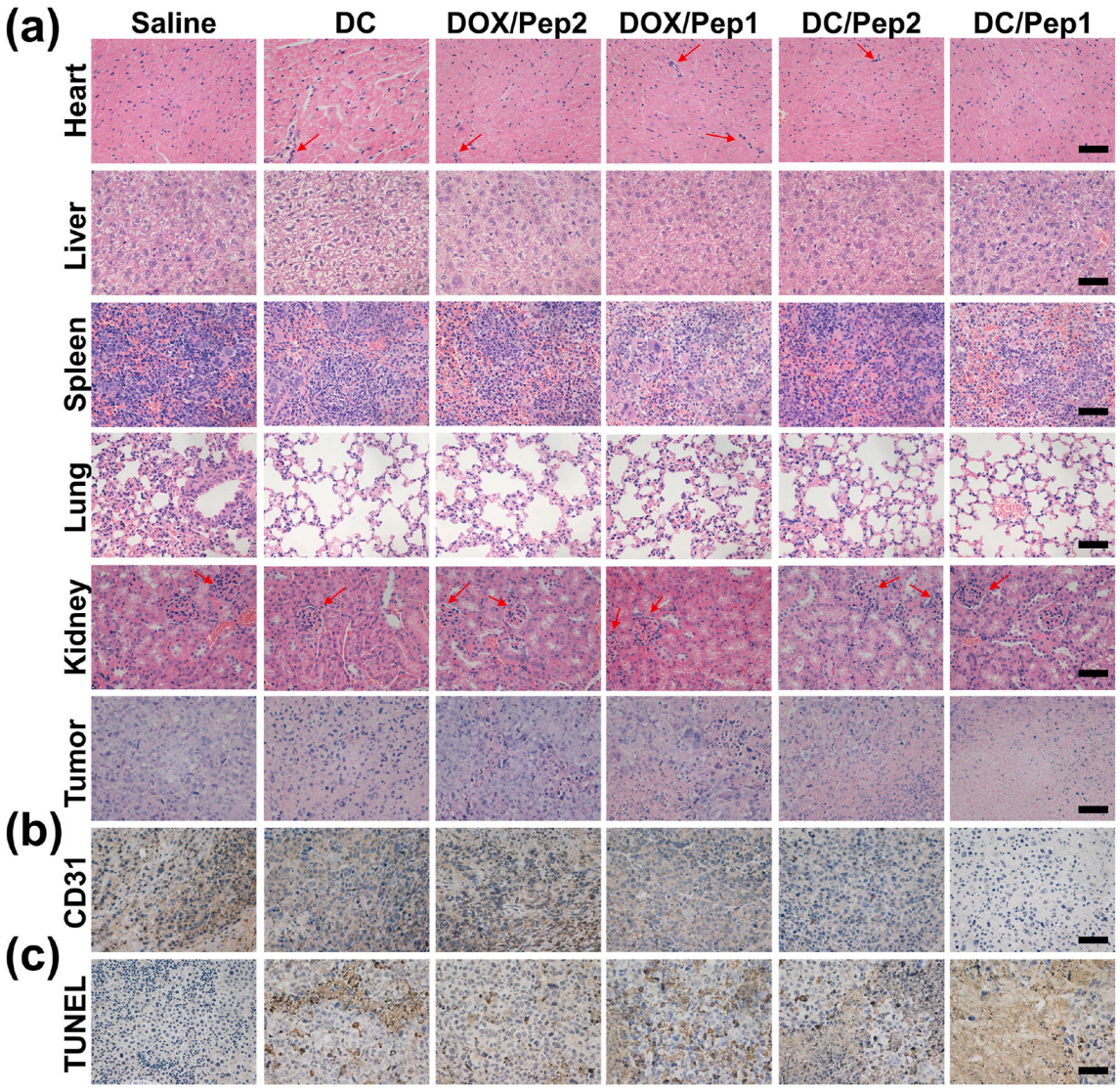

Fig. 7. Representative Histological Images of the Main Organs and Tumors of H22 Tumor-Bearing Mice after Different Treatments (Saline, DC, DOX/Pep2, DOX/Pep1, DC/Pep2, DC/Pep1). (a) After various treatments, the heart, liver, spleen, lung, kidney and tumor tissues of mice with tumors were examined using H&E staining. Scale bar: 30 μm. (b) Immunohistological staining for CD31 and (c) TUNEL staining of tumor sections treated with different medications. Scale bar: 30 μm.

addition, the morphologically transformable Pep1 nanocarriers enhanced drug retention.

Three days after receiving the final dose, the mice used in the experiment were sacrificed. The tumors were then collected, weighed, and photographed (Fig. 6a and b). After intravenous injection of DC/Pep1, the mouse tumor weights and volumes were decreased (Fig. 6c and d). The tumor inhibition efficiencies of DC, DOX/Pep2, DOX/Pep1, DC/Pep2, and DC/Pep1 were 26.8 %, 28.9 %, 35.9 %, 43.2 %, and 51.8 %, respectively. Tumor growth was rapid in the physiological saline group and was significantly inhibited in the DC/Pep1 group (Fig. 6e). The examination of the body weight indicated that there was an absence of notable alteration in the body weights of mice belonging to the DC/Pep1 group (Fig. 6f). This study confirmed that morphologically transformable DC/Pep1 NPs could effectively inhibit tumor growth.

Because of the strong cardiac and renal toxicity of DOX, H&E staining of the organs and tumor tissues of the mice was performed to observe the anticancer effect and adverse reaction of the different treatment groups. The mice in the DC, DOX/Pep2, DOX/Pep1, and DC/Pep2 groups exhibited different levels of harm to their hearts and kidneys. No significant pathological damage was seen in the heart tissues of the DC/Pep1 group after multiple doses (Fig. 7a). Tumor tissues stained with H&E showed that the DC/Pep1 group had a greater number of apoptotic tumor cells and appeared to have larger tumor areas of necrosis than the saline, DC, DOX/Pep2, DOX/Pep1 and DC/Pep2 groups (Fig. 7a). H&E staining demonstrated that DC/Pep1 has better antitumor properties and lower systemic toxicity.

CD31 is a common marker of tumor vascular endothelial cells [62,63] and is mainly used to indicate endothelial cell tissue and assess tumor vessels. The expression level of CD31 may indicate the rapidity of tumor growth [64,65]. Therefore, we chose CD31 to validate tumor neovascularization (Fig. 7b, Fig. S36). The results showed that the DC/Pep1 group had fewer CD31-positive regions and significantly fewer nuclei than the other groups. These findings align with the outcomes of the tumor vascular inhibition test. These experiments further demonstrate that DC/Pep1 can target tumor vessels to release drugs and inhibit neovascularization, thus inhibiting tumor progression.

TUNEL immunohistochemistry assays were utilized to observe the role of DC/Pep1 in the promotion of apoptosis (Fig. 7c, Fig. S37). In the DC/Pep1 group, we observed a greater presence of apoptotic zones within the tumor tissues, which were significantly disrupted and exhibited a considerable loss of nuclei.

To investigate the *in vivo* function of DC/Pep1, a mouse lung

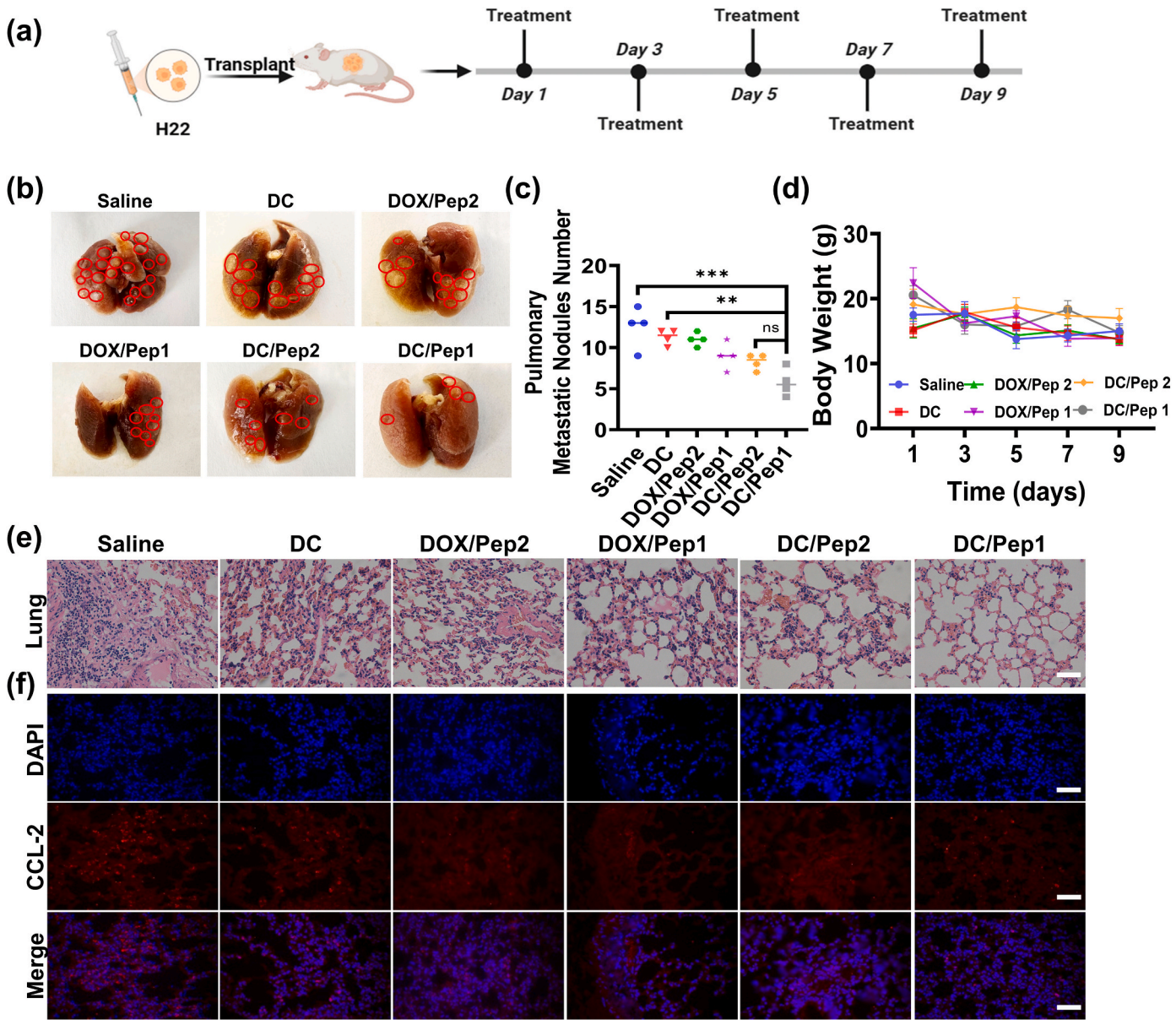

Fig. 8. Antimetastatic Effects of Different Preparations in the H22 Tumor Model. (a) *In vivo* antimetastasis assay in tumor-bearing mice. (b) Images of lung metastasis and (c) the count of nodules with lung metastases. $^{**}P < 0.01$; $^{***}P < 0.001$; ns, $P > 0.05$. (d) Body weight increase patterns of mice throughout the duration of the treatment. (e) H&E-stained lung sections. Scale bar: 50 μm. (f) The levels of CCL-2 in lung sections determined by immunofluorescence. Scale bar: 50 μm.

metastasis model was established (Fig. 8a). The average quantity of nodules in the DC/Pep1 group was notably lower than that in the saline, DC, DOX/Pep2, DOX/Pep1, and DC/Pep2 groups (Fig. 8b and c). The weights of the mice in the DC/Pep1 group remained relatively stable throughout the experiment (Fig. 8d). In the H&E-stained sections, the area of metastasis was smallest in the DC/Pep1 group (Fig. 8e). The lung metastasis experiment indicated that DC/Pep1 significantly inhibited the progression of lung metastasis.

CCL-2 promotes tumor cell migration, distant metastasis, and growth [66]. Immunofluorescence staining of lung tissue sections was used to observe the expression of CCL-2. The DC/Pep1 group exhibited a notable decrease in CCL-2 expression compared to the other groups (Fig. 8f, Fig. S38). Thus, DC/Pep1 may inhibit tumor lung metastasis by inhibiting CCL-2 expression.

In this study, morphologically transformable DC/Pep1 was successfully prepared, leading to enhanced utilization and prolonged retention of CUR and DOX within the tumor. The cellular uptake results showed that DC/Pep1 had a greater capacity to be taken up by HepG2 cells than free drugs. DC/Pep1 enhanced drug accumulation in HepG2 cells better than DC/Pep2, which may be related to the morphological transformation of DC/Pep1. The live imaging results showed that DiR and DiR/Pep2 were mainly distributed in the heart and kidney, while a large amount of DiR/Pep1 was enriched at tumor sites, and there was still significant fluorescence in tumor sites of mice in the DC/Pep1 group after 96 h. The tumor sizes in the DC/Pep1 group exhibited a notable decrease during the antitumor trials.

We examined the impact of DC/Pep1 on apoptosis (Caspase-3 expression) and angiogenesis inhibition in HepG2 cells. Apoptosis and WB assays indicated that the apoptosis rate in the DC/Pep1 group was highest. WB assay results additionally demonstrated an elevation in the expression level of Caspase-3 within this group, indicating that DC/Pep1 effectively promoted apoptosis of HepG2 cells. In an angiogenesis assay, DC/Pep1 significantly inhibited angiogenesis, and immunohistochemical staining of CD31 showed that DC/Pep1 could target blood vessels in microthrombi and release the encapsulated drug to inhibit angiogenesis. These results suggest that DC/Pep1 can synergistically treat HCC by

promoting apoptosis and inhibiting angiogenesis.

4. Conclusion

In conclusion, the self-assembling peptide nanodrug delivery system DC/Pep1 undergoes a morphological shift when exposed to an acidic environment to enhance drug retention and improve cancer therapy. To reduce toxic drug side effects and increase selective toxicity to tumor cells, the peptide vector incorporated a tumor microthrombus vascular targeting component in its design. DC/Pep1 delivers the drug to the vascular location of the tumor, inhibiting the generation of blood vessels in the tumor microenvironment. DC/Pep1 promotes and accelerates the process of apoptosis. The *in vivo* experimental results demonstrated that the retention of the drug at the tumor site was significantly enhanced, which may be related to the morphological transformation of DC/Pep1. Furthermore, DC/Pep1 demonstrated significant efficacy in suppressing tumor development and preventing the spread of cancer cells to the lungs. DC/Pep1 inhibits the growth and metastasis of liver cancer, which provides ideas for designing morphologically transformable drug-loaded systems for tumor therapy.

Author contributions

Conception and design: J. Bai. Development of methodology: Y. Liu, Y. Liu, X. Sun. Acquisition of data: Y. Liu, Y. Liu, X. Sun, Y. Wang. Analysis and interpretation of data: Y. Liu, X. Sun, Y. Wang, C. Du, J. Bai. Writing, review, and/or revision of the manuscript: Y. Liu, J. Bai.

Declaration of competing interest

The authors declare that they have no known competing financial interests or personal relationships that could have appeared to influence the work reported in this paper.

Data availability

Data will be made available on request.

Acknowledgments

This work was supported by the Natural Science Foundation of Shandong Province (ZR2023MC122).

Appendix A. Supplementary data

Supplementary data to this article can be found online at https://doi.org/10.1016/j.mtbio.2023.100903.

References

[1] H. Rumgay, M. Arnold, J. Ferlay, O. Lesi, C.J. Cabasag, J. Vignat, M. Laversanne, K. A. McGlynn, I. Soerjomataram, Global burden of primary liver cancer in 2020 and predictions to 2040, J. Hepatol. 77 (2022) 1598–1606.
[2] D. Anwanwan, S.K. Singh, S. Singh, V. Saikam, R. Singh, Challenges in liver cancer and possible treatment approaches, Biochim. Biophys. Acta, Rev. Cancer. 1873 (2020), 188314.
[3] I.V. Larionova, T. Liu, V. Riabov, D.M. Mossel, M.R. Patysheva, A.M. Kiselev, E. O. Kazakova, N.V. Cherdyntseva, J. Kzhyshkowska, 2026P - the clearance of EGF by tumor-associated macrophages is suppressed by chemotherapeutic agent cisplatin, Ann. Oncol. 30 (2019) v810.
[4] M. Zhang, H. Ma, X. Wang, B. Yu, H. Cong, Y. Shen, Polysaccharide-based nanocarriers for efficient transvascular drug delivery, J. Controlled Release 354 (2023) 167–187.
[5] A. Tahmasbi Rad, C.W. Chen, W. Aresh, Y. Xia, P.S. Lai, M.P. Nieh, Combinational effects of active targeting, shape, and enhanced permeability and retention for cancer theranostic nanocarriers, ACS Appl. Mater. Interfaces 11 (2019) 10505–10519.
[6] Q. Sun, X. Sun, X. Ma, Z. Zhou, E. Jin, B. Zhang, Y. Shen, E.A. Van Kirk, W. J. Murdoch, J.R. Lott, T.P. Lodge, M. Radosz, Y. Zhao, Integration of nanoassembly functions for an effective delivery cascade for cancer drugs, Adv. Mater. 26 (2014) 7615–7621.
[7] Z. Xu, D. Yang, T. Long, L. Yuan, S. Qiu, D. Li, C. Mu, L. Ge, pH-Sensitive nanoparticles based on amphiphilic imidazole/cholesterol modified hydroxyethyl starch for tumor chemotherapy, Carbohydr. Polym. 277 (2022), 118827.
[8] H.R. Jia, Y.X. Zhu, X. Liu, G.Y. Pan, G. Gao, W. Sun, X. Zhang, Y.W. Jiang, F.G. Wu, Construction of dually responsive nanotransformers with nanosphere-nanofiber-nanosphere transition for overcoming the size paradox of anticancer nanodrugs, ACS Nano 13 (2019) 11781–11792.
[9] E. Hinde, K. Thammasiraphop, H.T. Duong, J. Yeow, B. Karagoz, C. Boyer, J. J. Gooding, K. Gaus, Pair correlation microscopy reveals the role of nanoparticle shape in intracellular transport and site of drug release, Nat. Nanotechnol. 12 (2017) 81–89.
[10] W. Jia, R. Liu, Y. Wang, C. Hu, W. Yu, Y. Zhou, L. Wang, M. Zhang, H. Gao, X. Gao, Dual-responsive nanoparticles with transformable shape and reversible charge for amplified chemo-photodynamic therapy of breast cancer, Acta Pharm. Sin. B 12 (2022) 3354–3366.
[11] A. Farzin, S. Hassan, L.S. Moreira Teixeira, M. Gurian, J.F. Crispim, V. Manhas, A. Carlier, H. Bae, L. Geris, I. Noshadi, S.R. Shin, J. Leijten, Self-oxygenation of tissues orchestrates full-thickness vascularization of living implants, Adv. Funct. Mater. 31 (2021), 2100850.
[12] W. Jia, Y. Wang, R. Liu, X. Yu, H. Gao, Shape transformable strategies for drug delivery, Adv. Funct. Mater. 31 (2021), 2009765.
[13] C. Lin, F. Tong, R. Liu, R. Xie, T. Lei, Y. Chen, Z. Yang, H. Gao, X. Yu, GSH-responsive SN38 dimer-loaded shape-transformable nanoparticles with iRGD for enhancing chemo-photodynamic therapy, Acta Pharm. Sin. B 10 (2020) 2348–2361.
[14] R. Liu, Y. An, W. Jia, Y. Wang, Y. Wu, Y. Zhen, J. Cao, H. Gao, Macrophage-mimic shape changeable nanomedicine retained in tumor for multimodal therapy of breast cancer, J. Controlled Release 321 (2020) 589–601.
[15] Z. Gong, Y. Shi, H. Tan, L. Wang, Z. Gao, B. Lian, G. Wang, H. Sun, P. Sun, B. Zhou, J. Bai, Plasma amine oxidase-induced nanoparticle-to-nanofiber geometric transformation of an peptide for drug encapsulation and enhanced bactericidal activity, ACS Appl. Mater. Interfaces 12 (2020) 4323–4332.
[16] Z. Gong, B. Zhou, X. Liu, J. Cao, Z. Hong, J. Wang, X. Sun, X. Yuan, H. Tan, H. Ji, J. Bai, Enzyme-induced transformable peptide nanocarriers with enhanced drug permeability and retention to improve tumor nanotherapy efficacy, ACS Appl. Mater. Interfaces 13 (2021) 55913–55927.
[17] E. Boedtkjer, S.F. Pedersen, The acidic tumor microenvironment as a driver of cancer, Annu. Rev. Physiol. 82 (2020) 103–126.
[18] L. Feng, Z. Dong, D. Tao, Y. Zhang, Z. Liu, The acidic tumor microenvironment: a target for smart cancer nano-theranostics, Natl. Sci. Rev. 5 (2018) 269–286.
[19] X. Meng, Y. Yi, Y. Meng, G. Lv, X. Jiang, Y. Wu, W. Yang, Y. Yao, H. Xu, W. Bu, Self-enhanced acoustic impedance difference strategy for detecting the acidic tumor microenvironment, ACS Nano 16 (2022) 4217–4227.
[20] J. Yang, S. Liu, Z. Ye, L. Deng, A. Dong, J. Zhang, Multi-transformable nanocarrier with tumor extracellular acidity-activated charge reversal, size reduction and ligand reemergence for in vitro efficient doxorubicin loading and delivery, Mater. Sci. Eng. C 116 (2020), 111250.
[21] Z. Wu, B. Uhl, O. Gires, C.A. Reichel, A transcriptomic pan-cancer signature for survival prognostication and prediction of immunotherapy response based on endothelial senescence, J. Biomed. Sci. 30 (2023) 21.
[22] J.D. Martin, G. Seano, R.K. Jain, Normalizing function of tumor vessels: progress, opportunities, and challenges, Annu. Rev. Physiol. 81 (2019) 505–534.
[23] X. Li, M.W. Ullah, B. Li, H. Chen, Recent progress in advanced hydrogel-based embolic agents: from rational design strategies to improved endovascular embolization, Adv. Healthcare Mater. 12 (2023), e2202787.
[24] S. Hong, Q.-X. Huang, P. Ji, X. Pang, Y. Sun, S.-X. Cheng, X.-Z. Zhang, X. Chen, Vascular disrupting agent-induced amplification of tumor targeting and prodrug activation boosts anti-tumor efficacy, Sci. China: Chem. 65 (2022) 1994–2004.
[25] P. Nowak-Sliwinska, J.R. van Beijnum, C.J. Griffioen, Z.R. Huinen, N.G. Sopesens, R. Schulz, S.V. Jenkins, R.P.M. Dings, F.H. Groenendijk, E.J.M. Huijbers, V. Thijssen, E. Jonasch, F.A. Vyth-Dreese, E.S. Jordanova, A. Bex, R. Bernards, T. D. de Gruijl, A.W. Griffioen, Proinflammatory activity of VEGF-targeted treatment through reversal of tumor endothelial cell anergy, Angiogenesis 26 (2023) 279–293.
[26] L. Agemy, K.N. Sugahara, V.R. Kotamraju, K. Gujraty, O.M. Girard, Y. Kono, R. F. Mattrey, J.H. Park, M.J. Sailor, A.I. Jimenez, C. Cativiela, D. Zanuy, F.J. Sayago, C. Aleman, R. Nussinov, E. Ruoslahti, Nanoparticle-induced vascular blockade in human prostate cancer, Blood 116 (2010) 2847–2856.
[27] N. Zhang, B. Ru, J. Hu, L. Xu, Q. Wan, W. Liu, W. Cai, T. Zhu, Z. Ji, R. Guo, L. Zhang, S. Li, X. Tong, Recent advances of CREKA peptide-based nanoplatforms in biomedical applications, J. Nanobiotechnol. 21 (2023) 77.
[28] Y. Li, X. Zhao, X. Liu, K. Cheng, X. Han, Y. Zhang, H. Min, G. Liu, J. Xu, J. Shi, H. Qin, H. Fan, L. Ren, G. Nie, A bioinspired nanoprobe with multilevel responsive T (1) -weighted MR signal-amplification illuminates ultrasmall metastases, Adv. Mater. 32 (2020), e1906799.
[29] M. Ashrafizadeh, S. Mirzaei, M.H. Gholami, F. Hashemi, A. Zabolian, M. Raei, K. Hushmandi, A. Zarrabi, N.H. Voelcker, A.R. Aref, M.R. Hamblin, R.S. Varma, S. Samarghandian, I.J. Arostegi, M. Alzola, A.P. Kumar, V.K. Thakur, N. Nabavi, P. Makvandi, F.R. Tay, G. Orive, Hyaluronic acid-based nanoplatforms for Doxorubicin: a review of stimuli-responsive carriers, co-delivery and resistance suppression, Carbohydr. Polym. 272 (2021), 118491.
[30] S.N. Mohammad, Y.S. Choi, J.Y. Chung, E. Cedrone, B.W. Neun, M. A. Dobrovolskaia, X. Yang, W. Guo, Y.C. Chew, J. Kim, S. Baek, I.S. Kim, D. A. Fruman, Y.J. Kwon, Nanocomplexes of doxorubicin and DNA fragments for efficient and safe cancer chemotherapy, J. Controlled Release 354 (2023) 91–108.

[31] S. Li, F. Li, D. Wan, Z. Chen, J. Pan, X.J. Liang, A micelle-based stage-by-stage impelled system for efficient doxorubicin delivery, Bioact. Mater. 25 (2023) 783–795.
[32] J. Zhang, C. Li, Q. Xue, X. Yin, Y. Li, W. He, X. Chen, J. Zhang, R.L. Reis, Y. Wang, An efficient carbon-based drug delivery system for cancer therapy through the nucleus targeting and mitochondria mediated apoptotic pathway, Small Methods 5 (2021), 2100539.
[33] J. Zeien, W. Qiu, M. Triay, H.A. Dhaibar, D. Cruz-Topete, E.M. Cornett, I. Urits, O. Viswanath, A.D. Kaye, Clinical implications of chemotherapeutic agent organ toxicity on perioperative care, Biomed. Pharmacother. 146 (2022), 112503.
[34] Q. Gao, J. Feng, W. Liu, C. Wen, Y. Wu, Q. Liao, L. Zou, X. Sui, T. Xie, J. Zhang, Y. Hu, Opportunities and challenges for co-delivery nanomedicines based on combination of phytochemicals with chemotherapeutic drugs in cancer treatment, Adv. Drug Delivery Rev. 188 (2022), 114445.
[35] P.B. Araveti, A. Srivastava, Curcumin induced oxidative stress causes autophagy and apoptosis in bovine leucocytes transformed by Theileria annulata, Cell Death Discovery 5 (2019) 100.
[36] R. Daya, C. Xu, N.T. Nguyen, H.H. Liu, Angiogenic hyaluronic acid hydrogels with curcumin-coated magnetic nanoparticles for tissue repair, ACS Appl. Mater. Interfaces. 14 (2022) 11051–11067.
[37] M. Yang, L. Yu, R. Guo, A. Dong, C. Lin, J. Zhang, A modular coassembly approach to all-in-one multifunctional nanoplatform for synergistic codelivery of doxorubicin and curcumin, Nanomaterials 8 (2018) 167.
[38] Q. Jin, Y. Deng, X. Chen, J. Ji, Rational design of cancer nanomedicine for simultaneous stealth surface and enhanced cellular uptake, ACS Nano 13 (2019) 954–977.
[39] Y. Zhang, H. Cui, R. Zhang, H. Zhang, W. Huang, Nanoparticulation of prodrug into medicines for cancer therapy, Adv. Sci. 8 (2021), e2101454.
[40] J. Cao, X. Liu, X. Yuan, F. Meng, X. Sun, L. Xu, H. Li, Y. Liu, Z. Hong, J. Bai, Enzyme-induced morphological transformation of self-assembled peptide nanovehicles potentiates intratumoral aggregation and inhibits tumour immunosuppression, Chem. Eng. J. 454 (2023), 140466.
[41] J. Cao, X. Yuan, X. Sun, F. Meng, H. Li, Z. Hong, Y. Liu, X. Zhai, J. Ma, S. Peng, Y. Zhou, X. Liu, J. Hao, J. Bai, Matrix metalloproteinase-2-induced morphologic transformation of self-assembled peptide nanocarriers inhibits tumor growth and metastasis, ACS Mater. Lett. 5 (2023) 900–908.
[42] D. Hao, Z. Zhang, Y. Cheng, L. Cheng, Y. Ji, Rational design of ibuprofen-based redox-responsive anti-cancer polymeric drug delivery systems, J. Mater. Sci. 57 (2022) 11317–11331.
[43] D. Lin, L. Xiao, W. Qin, D.A. Loy, Z. Wu, H. Chen, Q. Zhang, Preparation, characterization and antioxidant properties of curcumin encapsulated chitosan/lignosulfonate micelles, Carbohydr. Polym. 281 (2022), 119080.
[44] D.E. Korenchan, R.R. Flavell, Spatiotemporal pH heterogeneity as a promoter of cancer progression and therapeutic resistance, Cancers 11 (2019) 1026.
[45] J. Li, Y. Kuang, J. Shi, J. Zhou, J.E. Medina, R. Zhou, D. Yuan, C. Yang, H. Wang, Z. Yang, J. Liu, D.M. Dinulescu, B. Xu, Enzyme-instructed intracellular molecular self-assembly to boost activity of cisplatin against drug-resistant ovarian cancer cells, Angew. Chem. 54 (2015) 13307–13311.
[46] D. Ingato, J.A. Edson, M. Zakharian, Y.J. Kwon, Cancer cell-derived, drug-loaded nanovesicles induced by sulfhydryl-blocking for effective and safe cancer therapy, ACS Nano 12 (2018) 9568–9577.
[47] K. Sasaki, J. Ishihara, A. Ishihara, R. Miura, A. Mansurov, K. Fukunaga, J. A. Hubbell, Engineered collagen-binding serum albumin as a drug conjugate carrier for cancer therapy, Sci. Adv. 5 (2019), eaaw6081.
[48] P.Y. Teo, W. Cheng, J.L. Hedrick, Y.Y. Yang, Co-delivery of drugs and plasmid DNA for cancer therapy, Adv. Drug Delivery Rev. 98 (2016) 41–63.
[49] E.C. Cho, J. Xie, P.A. Wurm, Y. Xia, Understanding the role of surface charges in cellular adsorption versus internalization by selectively removing gold nanoparticles on the cell surface with a I2/KI etchant, Nano Lett. 9 (2009) 1080–1084.
[50] X. Tao, Y. Xie, Q. Zhang, X. Qiu, L. Yuan, Y. Wen, M. Li, X. Yang, T. Tao, M. Xie, Y. Lv, Q. Wang, X. Feng, Cholesterol-Modified amino-pullulan nanoparticles as a drug carrier: comparative study of cholesterol-modified carboxyethyl pullulan and pullulan nanoparticles, Nanomaterials 6 (2016) 165.
[51] L. Chen, J.M. McCrate, J.C. Lee, H. Li, The role of surface charge on the uptake and biocompatibility of hydroxyapatite nanoparticles with osteoblast cells, Nanotechnology 22 (2011), 105708.
[52] A. Baoum, N. Dhillon, S. Buch, C. Berkland, Cationic surface modification of PLG nanoparticles offers sustained gene delivery to pulmonary epithelial cells, J. Pharmaceut. Sci. 99 (2010) 2413–2422.
[53] K. Lu, Z. Li, Q. Hu, J. Sun, M. Chen, CRPC membrane-camouflaged, biomimetic nanosystem for overcoming castration-resistant prostate cancer by cellular vehicle-aided tumor targeting, Int. J. Mol. Sci. 23 (2022) 3623.
[54] H.L. Ang, C.D. Mohan, M.K. Shanmugam, H.C. Leong, P. Makvandi, K.S. Rangappa, A. Bishayee, A.P. Kumar, G. Sethi, Mechanism of epithelial-mesenchymal transition in cancer and its regulation by natural compounds, Med. Res. Rev. 43 (2023) 1141–1200.
[55] Y.M. Hsu, Y.F. Chen, C.Y. Chou, M.J. Tang, J.H. Chen, R.J. Wilkins, J.C. Ellory, M. R. Shen, KCl cotransporter-3 down-regulates E-cadherin/beta-catenin complex to promote epithelial-mesenchymal transition, Cancer Res. 67 (2007) 11064–11073.
[56] F.J. Bock, E. Sedov, E. Koren, A.L. Koessinger, C. Cloix, D. Zerbst, D. Athineos, J. Anand, K.J. Campbell, K. Blyth, Y. Fuchs, S.W.G. Tait, Apoptotic stress-induced FGF signalling promotes non-cell autonomous resistance to cell death, Nat. Commun. 12 (2021) 6572.
[57] D. Bertheloot, E. Latz, B.S. Franklin, Necroptosis, pyroptosis and apoptosis: an intricate game of cell death, Cell. Mol. Immunol. 18 (2021) 1106–1121.
[58] C. Rogers, D.A. Erkes, A. Nardone, A.E. Aplin, T. Fernandes-Alnemri, E.S. Alnemri, Gasdermin pores permeabilize mitochondria to augment caspase-3 activation during apoptosis and inflammasome activation, Nat. Commun. 10 (2019) 1689.
[59] F. Abedi, S. Davaran, M. Hekmati, A. Akbarzadeh, B. Baradaran, S.V. Moghaddam, An improved method in fabrication of smart dual-responsive nanogels for controlled release of doxorubicin and curcumin in HT-29 colon cancer cells, J. Nanobiotechnol. 19 (2021) 18.
[60] B. Tavora, T. Mederer, K.J. Wessel, S. Ruffing, M. Sadjadi, M. Missmahl, B. N. Ostendorf, X. Liu, J.Y. Kim, O. Olsen, A.L. Welm, H. Goodarzi, S.F. Tavazoie, Tumoural activation of TLR3-SLIT2 axis in endothelium drives metastasis, Nature 586 (2020) 299–304.
[61] A. Jhaveri, V. Torchilin, Intracellular delivery of nanocarriers and targeting to subcellular organelles, Expet Opin. Drug Delivery 13 (2016) 49–70.
[62] J. Meng, Y. Liu, J. Han, Q. Tan, S. Chen, K. Qiao, H. Zhou, T. Sun, C. Yang, Hsp90β promoted endothelial cell-dependent tumor angiogenesis in hepatocellular carcinoma, Mol. Cancer 16 (2017) 72.
[63] Q. Wang, B. Qian, M. Schäfer, W. Groß, A. Mehrabi, E. Ryschich, Fluorescence-guided fiber-optic micronavigation using microscopic identification of vascular boundary of liver segment and tumors, Theranostics 10 (2020) 6136–6148.
[64] Y. Wang, L. Dong, H. Zhong, L. Yang, Q. Li, C. Su, W. Gu, Y. Qian, Extracellular vesicles (EVs) from lung adenocarcinoma cells promote human umbilical vein endothelial cell (HUVEC) angiogenesis through yes kinase-associated protein (YAP) transport, Int. J. Biol. Sci. 15 (2019) 2110–2118.
[65] C. Charpin, J.P. Dales, S. Garcia, S. Carpentier, A. Djemli, L. Andrac, M.N. Lavaut, C. Allasia, P. Bonnier, Tumor neoangiogenesis by CD31 and CD105 expression evaluation in breast carcinoma tissue microarrays, Clin. Cancer Res. 10 (2004) 5815–5819.
[66] S. Gening, T. Abakumova, T. Gening, IL-17A and CCL2 in blood serum and circulating neutrophils in patients with ovarian tumors, J. Clin. Oncol. 39 (2021), e17536.